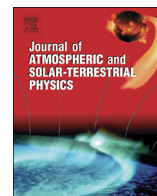




ELSEVIER

Contents lists available at ScienceDirect

Journal of Atmospheric and Solar-Terrestrial Physics

journal homepage: www.elsevier.com/locate/jastp

Observability of NEIALs with the Sondrestrom and Poker Flat incoherent scatter radars

R.G. Michell*, M. Samara

Southwest Research Institute, San Antonio, TX, USA

ARTICLE INFO

Article history:

Received 5 April 2012

Received in revised form

30 November 2012

Accepted 9 December 2012

Available online 4 January 2013

Keywords:

Incoherent scatter radar

PFISR

NEIALs

Sondrestrom

ABSTRACT

We present coordinated optical and radar observations using the Poker Flat Incoherent Scatter Radar (PFISR) in Alaska and the Sondrestrom radar in Greenland. Several cases were examined where intense, similar-looking dynamic auroral structures were observed in the magnetic zenith. The presence or absence of Naturally Enhanced Ion Acoustic Lines (NEIALs) was investigated in both sets of radar data. In all cases, the aurora exhibited small-scale (~ 0.1 – 1 km), dynamic features that were observed with both all-sky and narrow-field of view (19°) imagers. In all of the cases examined, the PFISR radar observed NEIALs while the Sondrestrom radar did not, despite similar auroral morphology. The main difference between the radars, namely the probing wave number, provides strong evidence for a limiting spatial scale of between 10 and 15 cm for the enhanced wave activity responsible for NEIALs. This has implications for constraining the models of NEIAL generation mechanisms.

© 2013 Elsevier Ltd. All rights reserved.

1. Introduction and background

Naturally Enhanced Ion Acoustic Lines (NEIALs) observed in radar data are interpreted to be backscatter from enhanced ion-acoustic wave activity. NEIALs were originally observed by Foster et al. (1988), with the Millstone Hill Incoherent Scatter Radar and subsequently observed with the European Incoherent Scatter (EISCAT) radars (such as Rietveld and Collis, 1991; Collis et al., 1991; Rietveld et al., 1996; Sedgemore-Schulthess et al., 1999; Ogawa et al., 2000, 2006; Grydeland et al., 2003, 2004; Strømme et al., 2005; Blixt et al., 2005; Lunde et al., 2007). These include observations made at the EISCAT Svalbard Radar (ESR) and the mainland radars near Tromsø. A connection between NEIALs and aurora was noticed early on Collis et al. (1991) and Rietveld and Collis (1991), but specifically combining auroral imaging with radar studies using the EISCAT radars was done more recently (Sedgemore-Schulthess et al., 1999; Grydeland et al., 2003, 2004; Blixt et al., 2005). These studies found correlations between the occurrence of aurora and the presence of NEIALs in the radar returns.

High spatial and temporal resolution auroral imaging was conducted with common volume observations of dayside NEIALs from the EISCAT ESR radar (Blixt et al., 2005) and nightside NEIALs from the Poker Flat Incoherent Scatter Radar (PFISR) (Michell et al., 2008, 2009; Michell and Samara, 2010). These

studies revealed that NEIALs, observed on the nightside, are associated with specific types of small-scale dynamic auroral forms. The EISCAT observations found NEIALs to be associated with “flaming” aurora and tall rayed auroral forms, indicative of large-fluxes of low energy electrons (Blixt et al., 2005). The PFISR observations found NEIALs to occur with dynamic small-scale auroral structures, particularly associated with sub-storm onset aurora containing thin rayed arcs. Additionally using PFISR, Michell et al. (2008) found NEIALs to occur at the poleward edge of a large-scale active auroral arc system.

To date, no observations of NEIALs have been confirmed with the Sondrestrom radar despite often observing dynamic polar-cap boundary aurora containing tall, rayed auroral arcs. In the study presented here, a specific comparison is made between the auroral features observed with high resolution at both PFISR and Sondrestrom. These auroral observations are then used to compare and contrast the presence and absence of NEIALs in the radar data.

Such a comparison could test the observability of NEIALs with the Sondrestrom radar, when it measures the same type of dynamic, tall-rayed aurora that has been shown to consistently produce NEIALs in both the PFISR and EISCAT radars. Understanding this connection would have implications for the scale sizes over which the enhanced wave activity and instabilities occur. This can then be used to constrain the modeling of the generation mechanisms of NEIALs, which is still an unresolved issue.

Cabrit et al. (1996) used the two EISCAT radars to examine the difference between NEIALs observed with the UHF (933 MHz) and

* Corresponding author. Tel.: +1 210 522 2279.

E-mail address: rmichell@swri.edu (R.G. Michell).

the VHF (224 MHz) in order to examine k -vector effects. We present an extension of this type of analysis using the Sondrestrom radar at an even higher frequency (1290 MHz).

Recent modeling efforts of possible NEIAL generation mechanisms include, enhanced ion-acoustic waves being driven by electrostatic ion cyclotron waves (Bahcivan and Cosgrove, 2008) and electron beam driven enhanced Langmuir waves, which decay into ion-acoustic waves (Kontar and Pécseli, 2005). Daldorff et al. (2007) modeled electron acoustic and plasma waves caused by cold electron beams, which subsequently produce asymmetric ion lines. Strømme et al. (2005), using EISCAT, found observational evidence for a connection between enhanced Langmuir waves, as evidenced by enhanced plasma line power in the radar data, and NEIALs. This showed that naturally enhanced Langmuir waves can generate enhanced ion-acoustic waves, broadening the possible NEIAL generation mechanisms to also include processes that can generate enhanced Langmuir waves. The electron beam driven Langmuir turbulence model, originally proposed by Forme (1993), is another plausible mechanism. This was recently modeled further by Guio and Forme (2006), for both the weak and strong Langmuir turbulence cases.

2. Method

Auroral imaging and radar data are discussed for a total of five auroral events, three that occurred over Sondrestrom, Greenland and two that occurred over Poker Flat, Alaska. The Sondrestrom radar (66.98°N, 50.95°W, geographic) is located near the poleward edge of the statistical auroral oval, therefore dynamic polar cap boundary aurorae are often observed in the local magnetic zenith. The PFISR radar (65.12°N, 147.43°W, geographic), adjacent to the Poker Flat Research Range in Fairbanks, AK is located near the equatorward edge of the statistical auroral oval, therefore dynamic polar cap aurorae and substorm onset aurora are observed in the local magnetic zenith during geomagnetically disturbed times. Fig. 1 shows the locations of PFISR and Sondrestrom relative to the statistical auroral oval.

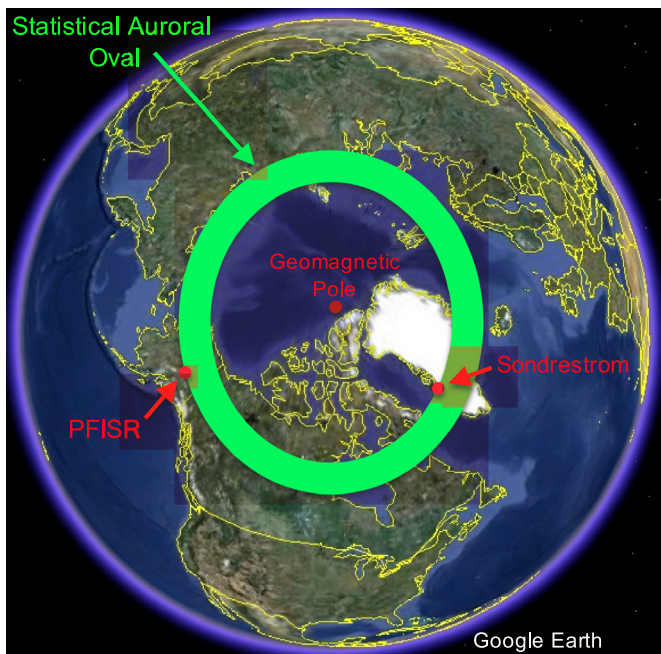


Fig. 1. Map of the statistical auroral oval showing the relative locations of PFISR and the Sondrestrom radar. Map courtesy of Google Earth.

Sondrestrom is a dish radar and has an operating frequency of 1290 MHz, therefore a Bragg scattering scale size of 11 cm. PFISR is a phased-array radar at 449 MHz and has a Bragg scattering scale size of 33 cm. The comparison between the two radars is made for observations made in the magnetic zenith only. Both radars used long, uncoded pulses (450 μ s), in order to gain maximum spectral information from the F-region ionosphere. Such a long pulse leads to altitude smearing of ~ 70 km. Both radars have similar sized beam widths, $\sim 1^\circ$ for PFISR and $\sim 0.5^\circ$ for Sondrestrom, both illuminating small areas in the ionosphere. The typical operating power of the two radars is also comparable, around 2 MW. Therefore the main point of comparison between Sondrestrom and PFISR is their operating frequency or equivalently their probing wave numbers.

The imagers used to make the auroral observations were Andor Ixon DU-888 EMCCD imagers. These have a 1024×1024 pixel chip, with internal binning capabilities that allow tradeoffs between temporal and spatial resolution. In each case, one was equipped with a narrow ($19^\circ \times 19^\circ$) field of view lens and one was equipped with an all-sky field of view lens. The CCDs were cooled to -70°C to reduce thermal noise and were set to 4×4 binning, resulting in a 256×256 image at 31 frames per second (~ 30 ms exposure time). This configuration was chosen because it provides adequate temporal resolution while still keeping a reasonable angular resolution of 0.058° per pixel or approximately 100 m per pixel for the narrowfield and 800 m–1000 m per pixel for the all-sky in the vicinity of the zenith, assuming auroral emissions at 100 km altitude. The narrowfield imagers were pointed at the magnetic zenith, which is near the center of the all-sky images for both Sondrestrom and Poker Flat. All of the auroral images presented here are oriented such that North is at the bottom and East is to the right.

3. Observations

In order to identify NEIALs in the radar data, we make use of their two main characteristics. First is the large backscattered power, which can be several orders of magnitude greater than the background incoherent scatter. NEIALs can be distinguished from satellite or other non-geophysical hard target scattering by examining the spectra of the enhanced power. NEIALs have the enhanced power at either or both of the ion acoustic shoulders, while satellites or space debris will have power near zero-Doppler shift.

For the comparison presented below, we first identify potential NEIALs based on enhanced returned power at times of active aurora. The potential NEIALs are then verified by examining the spectra of the enhanced returns. All the electron density profiles shown, both with and without NEIALs, are calculated directly from the scaled returned power. The main point for the comparison made here is solely the identification of NEIALs and therefore a full spectral fitting to get electron density is not needed. These radar data are integrated into 5 s periods and most of the NEIALs observed occur in only 1 or 2 of these 5 s periods and therefore show up as very localized in time. NEIALs typically occur in more than one ~ 70 km range gate, although they can occur in only one. This altitude extent criteria can also be used to rule out satellites and space debris, which only occur in one range gate.

3.1. Sondrestrom

An imaging campaign, lasting several months, was conducted at the Sondrestrom radar. Three nights in early April of 2011, with clearly active, rayed aurora are presented here. The radar shows clear enhancements in the E- and F-regions ionospheric density

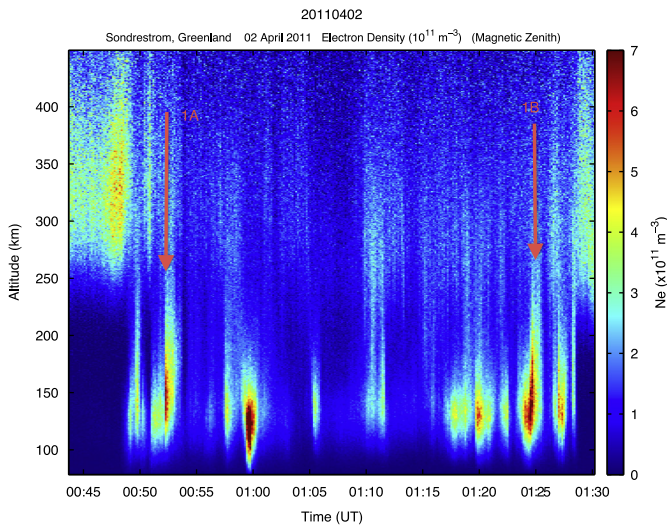


Fig. 2. Sondrestrom electron density (10^{11} m^{-3}) covering a time period of ~ 50 min on 02 April 2011, where active dynamic auroral structures were observed inside the radar beam. The red arrows, labeled 1A and 1B denote the times of the auroral images shown in Fig. 3. (For interpretation of the references to color in this figure caption, the reader is referred to the web version of this article.)

due to the electron precipitation, but no NEIAL features are observed. All three events shown occurred in the midnight sector, with magnetic midnight near 02:00 UT. Several other nights were examined and no NEIAL features have yet been observed in the Sondrestrom data.

Fig. 2 shows the electron density for 02 April 2011 as a function of altitude and time from the Sondrestrom radar, covering a period of about 50 min. For all three events, the radar was stationary and centered on the magnetic zenith. The electron density enhancements associated with the aurora can be seen to extend from less than 100 km to near 250 km altitude, in a smoothly varying manner and do not show any abrupt enhancements in power, indicative of NEIALs. The two red arrows on Fig. 2, labeled 1A and 1B, denote the times of the auroral images shown in Fig. 3. The first time, labeled 1A, (near 00:52 UT) corresponds to the top row of images in Fig. 3, with the all-sky image on the left and the narrowfield image on the right. The small red circle near the center of the all-sky image denotes the location of the narrowfield image. In this and all subsequent narrowfield images, the magnetic zenith (radar beam location) is located near the center of the narrowfield image and is approximately 1° wide (~ 1 km at 100 km altitude). The red circles on the narrowfield images denote the approximate locations of the radar beam at 100 km altitude. The black vertical line on the narrowfield image is saturation caused from the lidar beam that was also operating at Sondrestrom at this time. These imagers were recording in white-light (no filters) and the aurora was bright and actually saturated the imagers a few times, for which the data are set to 0 (black). In both cases, narrow (~ 1 km) auroral structures were observed to be highly dynamic with twisting and folding about the magnetic field. The field-aligned ray structure can be clearly seen in the bottom row of images, taken near 01:25 UT, labeled 1B.

The next example, from 03 April 2011, also shows strong enhancements in the electron density due to the auroral electron precipitation. Fig. 4 shows the Sondrestrom electron density for 03 April 2011 as a function of altitude and time, covering a period of about 30 min. Similarly, the enhancement in electron density is smoothly varying in both altitude and time and does not show any NEIAL-like enhancements. The auroral images taken at 02:24 UT (denoted by the red arrow (1C) in Fig. 4) are shown in Fig. 5.

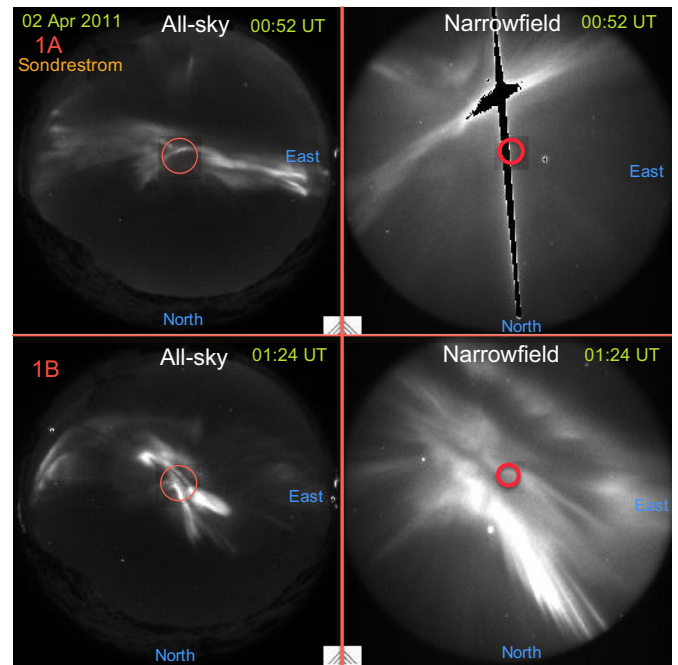


Fig. 3. Auroral images from Sondrestrom (02 April 2011), taken at the times denoted by the red arrows in Fig. 2. The all-sky images are on the left with their corresponding narrowfield images on the right. The red circle on the all-sky image is the location of the narrowfield. The red circles on the narrowfield images denote the locations of the radar beam at 100 km altitude. The top row (1A) was taken at 00:52 UT (22:52 MLT) and the bottom row (1B) at 01:24 UT (23:24 MLT). The dark vertical line on the narrowfield image is interference from the lidar beam. The data are set to 0 when saturated. (For interpretation of the references to color in this figure caption, the reader is referred to the web version of this article.)

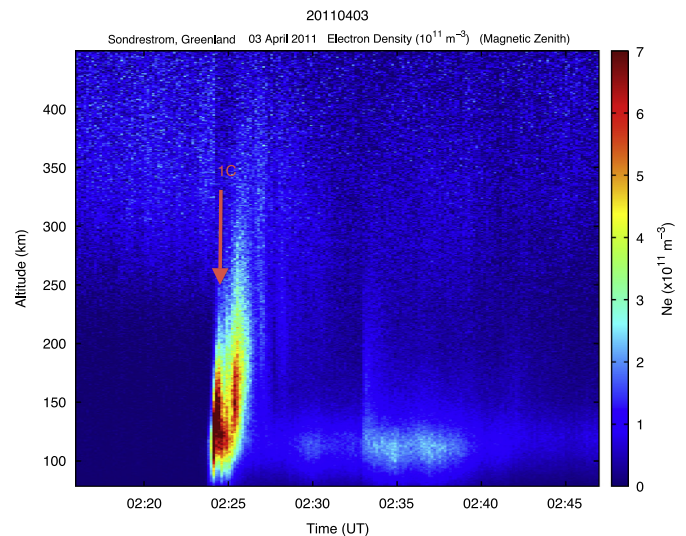


Fig. 4. Sondrestrom electron density (10^{11} m^{-3}) covering a time period of ~ 30 min on 03 April 2011, where active dynamic auroral structures were observed inside the radar beam. The red arrow, labeled 1C, denotes the time of the auroral images shown in Fig. 5. (For interpretation of the references to color in this figure caption, the reader is referred to the web version of this article.)

The all-sky image (left) shows an active, rayed auroral arc passing through zenith at this time and the narrowfield image (right) shows the dynamic, small-scale structures. The tall ray structure (150 km–300 km altitude) of the aurora is consistent with energy dispersed electron precipitation, with significant fluxes of lower energy (500 eV–2 keV) electrons (Rees, 1963).

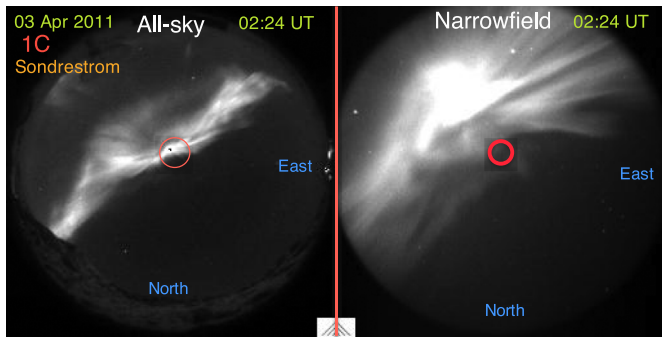


Fig. 5. Auroral images from Sondrestrom (03 April 2011), taken at the time denoted by the red arrow (1C) in Fig. 4. The all-sky image is on the left with its corresponding narrowfield image on the right. The red circle on the all-sky image is the location of the narrowfield. The red circle on the narrowfield image denotes the location of the radar beam at 100 km altitude. These images were taken at 02:24 UT (00:24 MLT). (For interpretation of the references to color in this figure caption, the reader is referred to the web version of this article.)

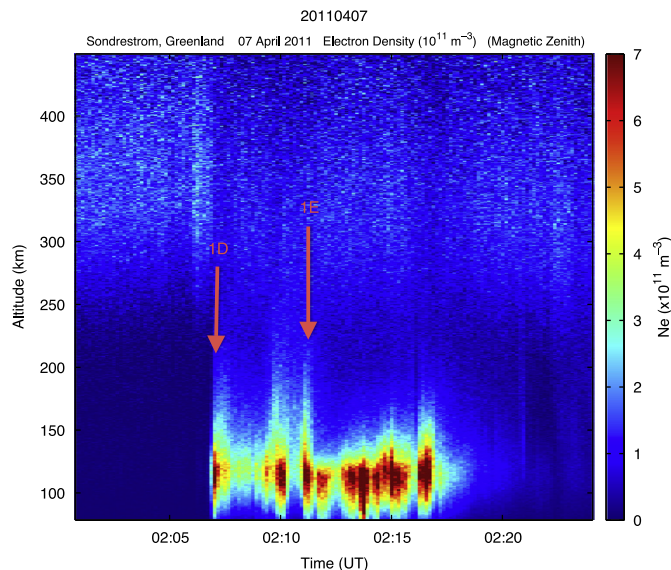


Fig. 6. Sondrestrom electron density (10^{11} m^{-3}) covering a time period of ~ 30 min on 07 April 2011, where active dynamic auroral structures were observed inside the radar beam. The red arrows, labeled 1D and 1E denote the times of the auroral images shown in Fig. 7. (For interpretation of the references to color in this figure caption, the reader is referred to the web version of this article.)

Fig. 6 shows the electron density from Sondrestrom for the auroral event that occurred on 07 April 2011, in the same format as Fig. 4. This case is slightly different from the others in that the electron density enhancement is primarily at lower altitudes (100 km–150 km), with some enhancement extending upwards to near 200 km altitude. This is indicative of electron precipitation with a larger characteristic energy (2 keV–10 keV) than in the other two cases (Rees, 1963). The auroral structures associated with these enhancements are shown in Fig. 7, where the top row of images corresponds to the red arrow labeled 1D in Fig. 6 and the bottom row to the red arrow labeled 1E. Again the aurora displays highly structured rapid moving small-scale features.

3.2. Poker flat

The increase in auroral activity in 2011 and 2012 has correspondingly increased the occurrence of dynamic aurora over the

PFISR radar, resulting in more NEIALs being observed along with their corresponding auroral structure. NEIALs typically occur in the PFISR data when the dynamic auroral structures associated with the polar cap boundary or substorm onset are in the magnetic zenith (Michell et al., 2008, 2009; Michell and Samara, 2010; Akbari et al., 2012; Isham et al., 2012). Two example cases are presented for comparison to the Sondrestrom data.

The first PFISR example is from 01 March 2011 and shows one of the largest amplitude NEIAL events observed with PFISR to date. These NEIAL returns also extend to high altitudes of up to 600 km. Fig. 8 shows the electron density from PFISR for this event, in the same format as the Sondrestrom radar data, only extending up to 700 km instead of 450 km in altitude. The actual electron density enhancements associated with the auroral precipitation can be seen between 100 km and 250 km altitude. The strongest NEIAL enhancements can be seen near 10:06 UT, when the poleward edge of the auroral oval passed into the magnetic zenith at substorm onset. The two red arrows, labeled 2A and 2B, denote the times of the auroral images shown in Fig. 10. The aurora at these times showed dynamic rayed structure. Fig. 10 shows two sets of images, with the top row, labeled 2A, taken at 10:05:30 UT (22:45 MLT) and the bottom row, labeled 2B, taken at 10:06:15 UT (22:46 MLT). The small red circle marked near the center of the all-sky denotes the location of the narrowfield image. The all-sky images (~ 1 s exposure time) on the left are taken with a 557.7 nm filter and therefore show the overall arc structure, which is highly twisted and structured. The narrowfield images on the right are taken with a BG3 glass filter in order to best view the rapid motions by targeting only the prompt emissions. In addition, the strongest NEIALs occur when the poleward edge of the aurora is in the magnetic zenith. The narrowfield images (30 ms exposure time) on the right show the dynamic, small-scale (< 1 km) features with field-aligned ray structure.

Fig. 9 shows the spectra for the two NEIALs labeled 2A and 2B in Fig. 8. The spectral and altitude structure of the NEIALs changes rapidly on short time scales (seconds). The NEIAL at 2A has both shoulders strongly and equally enhanced, while the NEIAL at 2B has the down-shifted shoulder much more strongly enhanced and extending to higher altitudes than the upshifted shoulder. The majority of NEIALs observed with PFISR so far have been confined to low altitudes (≤ 400 km), but these NEIALs extend up to fairly high altitudes of around 600 km.

Fig. 11 shows the PFISR electron density for the second example, 28 September 2011 as a function of altitude and time, covering a period of about 30 min. In this example, the main ionization occurs between 100 km and 200 km in altitude and the NEIAL features occur over a lower altitude range, mostly between 200 km and 300 km altitude. The strong returns in one range gate between 600 km and 700 km altitude are likely range aliased satellite returns and are thus not geophysical. The two red arrows, labeled 2C and 2D, denote the two times where example all-sky auroral images are shown in Fig. 13. The top image, labeled 2C, shows an active auroral structure with thin arcs and folds taken at 06:07 UT (18:47 MLT). The bottom image, labeled 2D, was taken at 06:26 UT (19:06 MLT) and shows the overall arc structure moving to the North with dynamic small-scale features in the magnetic zenith, which is denoted by a red box.

Fig. 12 shows the spectra for the two NEIALs labeled 2C and 2D in Fig. 11. The spectral and altitude structures of these NEIALs are significantly different from NEIALs 2A and 2B. These have the power confined to low altitudes, consistent with most of the previously reported NEIALs observed with PFISR. The power is also spread throughout the entire range between the ion-acoustic peaks.

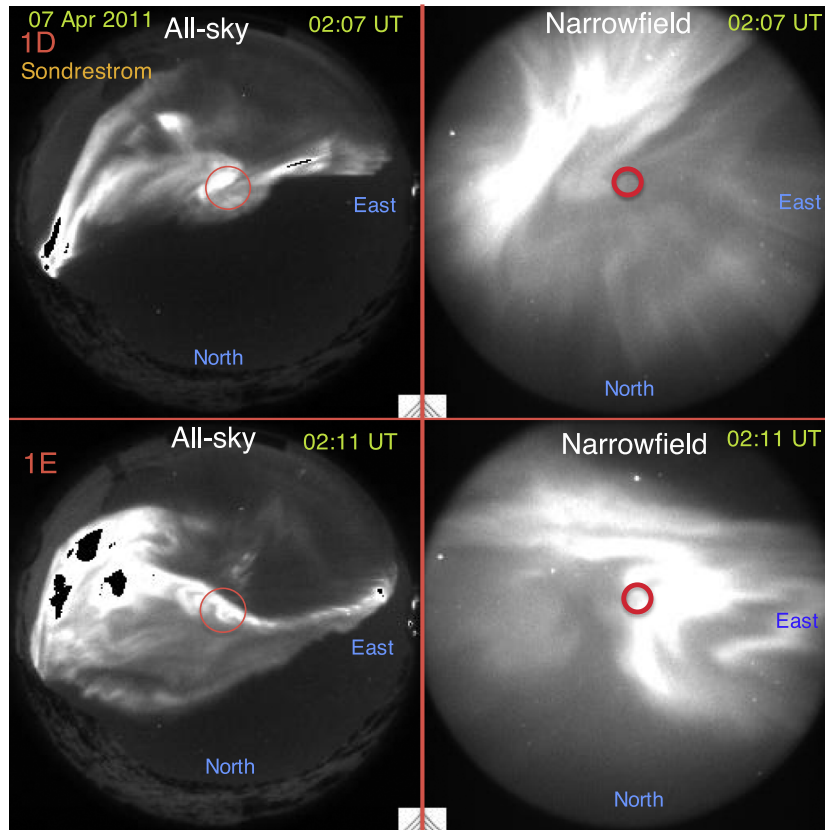


Fig. 7. Auroral images from Sondrestrom (07 April 2011), taken at the times denoted by the red arrows in Fig. 6. The all-sky images are on the left with their corresponding narrowfield images on the right. The red circle on the all-sky image is the location of the narrowfield. The red circles on the narrowfield images denote the locations of the radar beam at 100 km altitude. The top row (1D) was taken at 02:07 UT (00:07 MLT) and the bottom row (1E) at 02:11 UT (00:11 MLT). The black on the all-sky images are where the imager saturated and the data were set to 0. (For interpretation of the references to color in this figure caption, the reader is referred to the web version of this article.)

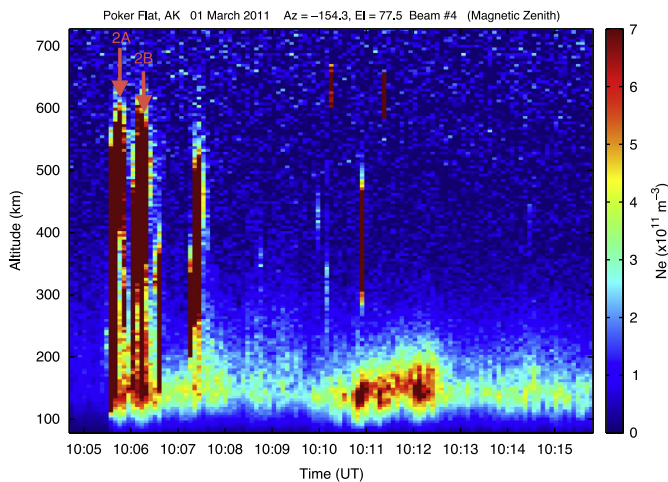


Fig. 8. PFISR electron density (10^{11} m^{-3}) covering a time period of ~ 10 min on 01 March 2011, where active dynamic auroral structures were observed inside the radar beam. The red arrows, labeled 2A and 2B, denote the times of the auroral images shown in Fig. 10. (For interpretation of the references to color in this figure caption, the reader is referred to the web version of this article.)

4. Discussion

The three auroral examples from Sondrestrom and the two examples from PFISR show that during geomagnetically active times, the aurorae show very similar morphological features and

incoherent radar backscatter at both sites. However, there is a distinct difference in the non-thermal radar backscatter (NEIAL) features observed with the two radars.

The events chosen for comparison all occurred near the equinoxes, although NEIALs are observed with PFISR throughout the entire winter auroral season. In order to make a consistent comparison, the active aurora that occurred near the vernal equinox at Sondrestrom, was compared to active aurora that occurred near both the vernal and autumnal equinoxes at PFISR.

There are several pieces of evidence leading to conclusion that the data presented in Figs. 8 and 11 are indeed NEIALs in the PFISR data. The first and most obvious is the much higher returned power, an order of magnitude or more above the background incoherent scatter at the same altitude. Secondly, examining the raw radar data, reveals the power is coming from a large range of altitudes, and is highly variable within the 5 s integration time of the electron density data shown. This is inconsistent with backscatter from hard targets such as satellites or space debris as those produce consistent returns at a constant altitude. Lastly and importantly, the spectra of the returned power reveal that the enhancements occurred at the two ion acoustic peaks ($\pm 6\text{--}8$ kHz for PFISR) for the 2A and 2B events and mostly between the ion acoustic peaks for events 2C and 2D, which also were confined to low altitudes (≤ 300 km).

Based on the similar auroral morphology at Sondrestrom and PFISR, there appears to be a lack of NEIALs observed with the Sondrestrom radar, or at least a much reduced occurrence frequency. This suggests a limiting scale size for the enhanced wave activity responsible for causing NEIALs. Previous observations with

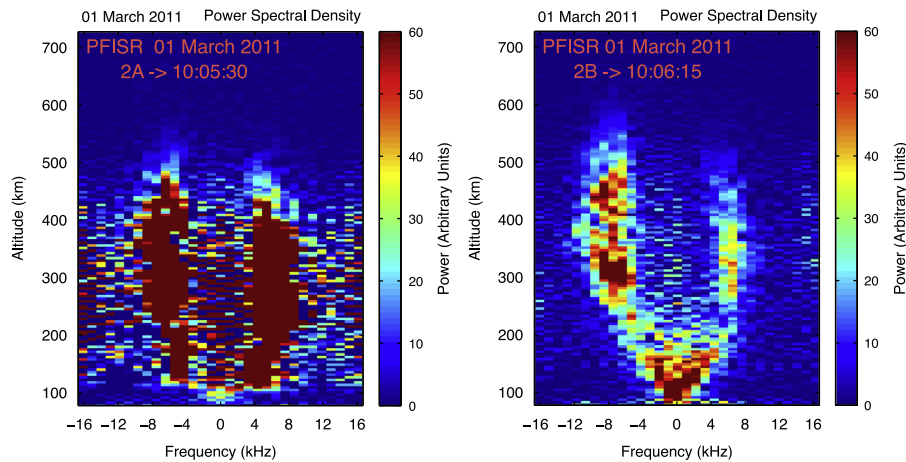


Fig. 9. The power spectral density as a function of altitude and frequency for the two NEIALs labeled (2A and 2B) in Fig. 8.

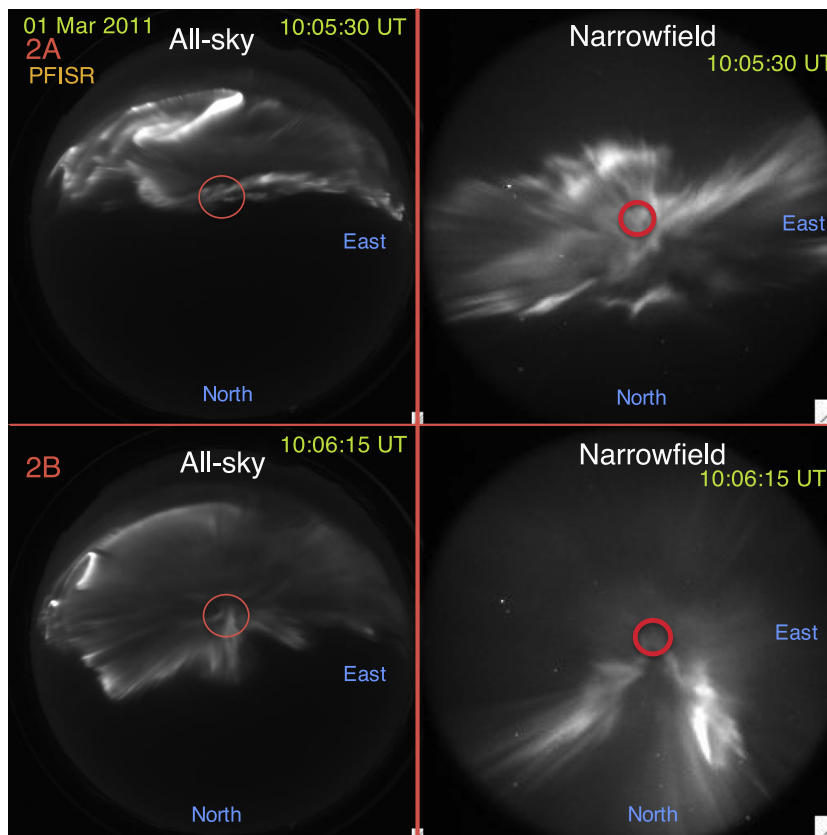


Fig. 10. Auroral images from Poker Flat (01 March 2011), taken at the times denoted by the red arrows in Fig. 8. The all-sky images are on the left with their corresponding narrowfield images on the right. The red circle on the all-sky image is the location of the narrowfield. The red circles on the narrowfield images denote the locations of the radar beam at 100 km altitude. The top row (2A) was taken at 10:05:30 UT (22:45 MLT) and the bottom row (2B) at 10:06:15 UT (22:46 MLT). (For interpretation of the references to color in this figure caption, the reader is referred to the web version of this article.)

the other high-latitude ISRs have found the presence of NEIALs for a range of radar wavelengths. [Forme and Fontaine \(1999\)](#) found NEIALs in the data from the 224 MHz EISCAT VHF radar. NEIALs have been observed in the data from the ESR radar at 500 MHz ([Sedgemore-Schulthess et al., 1999](#); [Ogawa et al., 2000](#); [Grydeland et al., 2004](#)). NEIALs have also been observed in the data from the EISCAT Tromsø UHF radar at 933 MHz ([Rietveld and Collis, 1991](#)). These observations are summarized in [Table 1](#), which shows the main high latitude radars and their specifications.

Another major difference between the PFISR and Sondrestrom radars is their geomagnetic latitude. PFISR is near the equatorward edge of the auroral oval (66.1°), while Sondrestrom (74.2°) is near the poleward edge of the auroral oval (See [Fig. 1](#)). Therefore, it could be argued that they are likely to observe different types of aurora and this could potentially account for the difference in NEIAL observations. However, this is not the case, as dynamic aurora with similar morphology is observed at both radars. In addition, observations made with the other high latitude

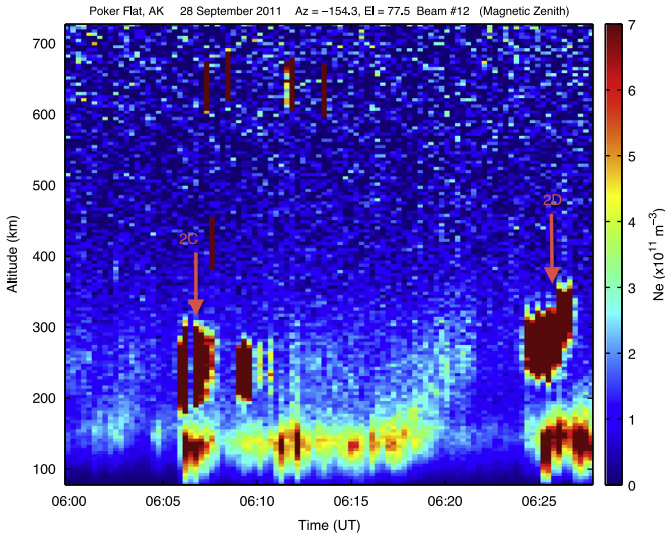


Fig. 11. PFISR electron density (10^{11} m^{-3}) covering a time period of ~ 30 min on 28 September 2011, where active dynamic auroral structures were observed inside the radar beam. The red arrows, labeled 2C and 2D, denote the times of the auroral images shown below.

ISRs (EISCAT) find the existence of NEIALs and active auroral structures at magnetic latitudes both above and below that of Sondrestrom. This lends further support to the idea that the enhanced wave activity responsible for NEIALs does occur in the aurora over Sondrestrom, but the radar there is not effectively scattering from it due to its smaller probing wave number. Table 1 shows that the EISCAT UHF and VHF radars are at nearly the same geomagnetic latitude as PFISR and NEIALs have been reported from all of these (Rietveld and Collis, 1991; Forme and Fontaine, 1999; Michell et al., 2008, 2009; Michell and Samara, 2010; Akbari et al., 2012; Isham et al., 2012). In addition, the ESR radar in Svalbard is at a slightly higher magnetic latitude (75.2°) than Sondrestrom and several cases have been reported in the literature where NEIALs have been observed using the ESR (Sedgemore-Schulthess et al., 1999; Ogawa et al., 2000; Grydeland et al., 2004).

The lack of NEIALs in the Sondrestrom data actually presents an advantage for doing incoherent scatter science. The radar data from PFISR shown in Figs. 8 and 11, show that the NEIALs can actually create significant interference to the derived radar parameters. In particular, these features occur when the aurora is the most dynamic and active, which is exactly when the derived radar parameters would be of most use for understanding the actual physics occurring. For example, Fig. 4 shows the Sondrestrom

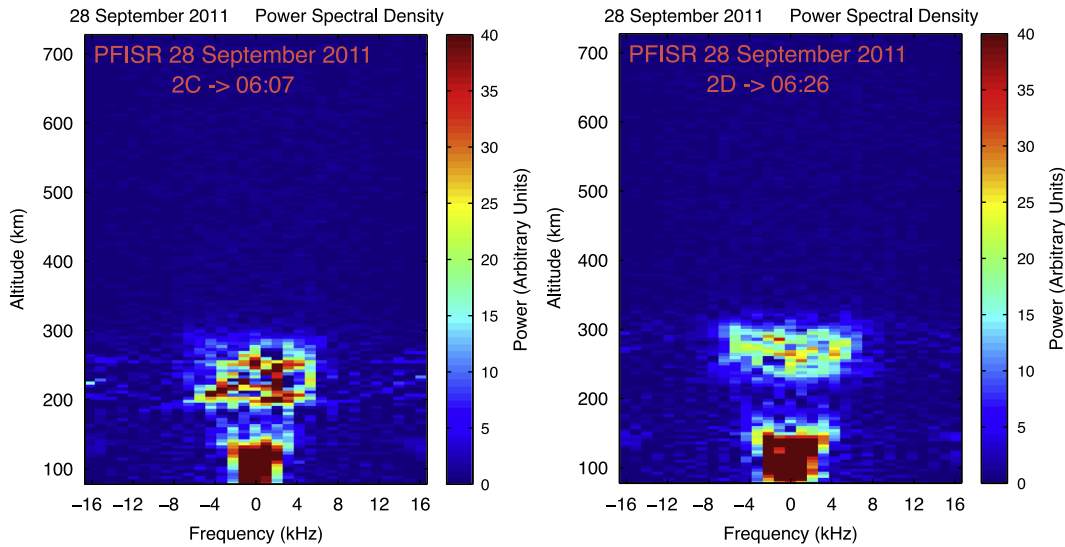


Fig. 12. The power spectral density as a function of altitude and frequency for the two NEIALs labeled (2C and 2D) in Fig. 11.

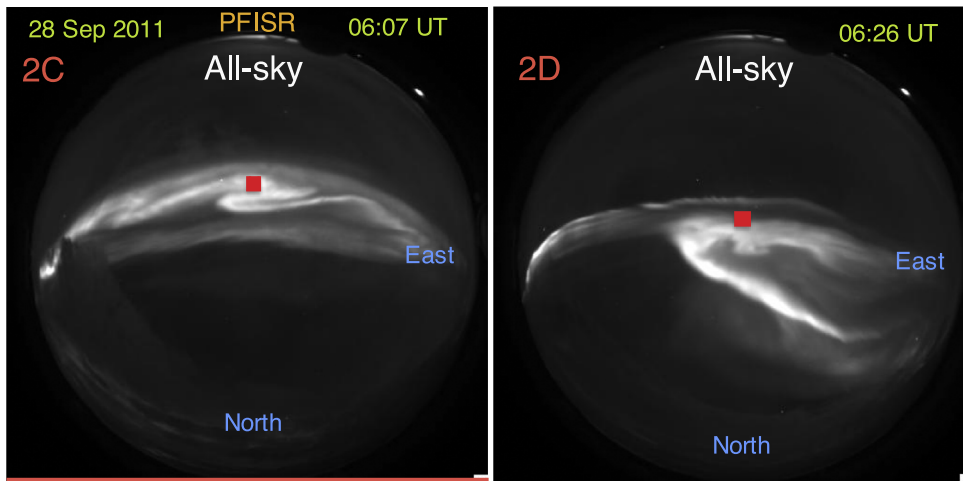


Fig. 13. All-sky images from Poker Flat (28 September 2011), taken at the times denoted by the red arrows, labeled 2C and 2D in Fig. 11. These imagers were recording in white-light (no filters). The top image (2C) was taken at 06:07 UT (18:47 MLT) and the bottom image (2D) at 06:26 UT (19:06 MLT). The magnetic zenith (radar beam location) is denoted by a red box. (For interpretation of the references to color in this figure caption, the reader is referred to the web version of this article.)

Table 1

Summary of the characteristics for the main high latitude radars, specifically the operating frequency, the Bragg scattering scale length ($\lambda/2$), the magnetic latitude and whether NEIALs have been observed with them or not.

Radar	Freq. (MHz)	$\lambda/2$ (cm)	Mag. lat. (deg)	Beamwidth (deg)	NEIALs
EISCAT VHF	224	67	66.2	1.5	Yes
PFISR	449	33	66.1	1	Yes
ESR	500	30	75.2	0.6	Yes
EISCAT UHF	933	16	66.2	0.5	Yes
Sondrestrom	1290	11	74.2	0.5	No (not yet?)

radar data varying smoothly without any strong NEIALs, allowing an accurate determination of the height and magnitude of the electron density enhancement associated with the observed auroral structures.

It is known that NEIALs can be associated with enhanced plasma lines in the radar data (Strømme et al., 2005). Recent modeling efforts also offer strong support for Langmuir turbulence occurring in the space plasma environment (Guio and Forme, 2006; Isham et al., 2012). Therefore it is possible that enhanced plasma lines could be observed with the Sondrestrom radar during these active times. In this case the enhanced Langmuir waves could result in enhanced plasma lines in the radar data, but when the Langmuir waves decay into ion-acoustic waves, the resulting scale size of the ion-acoustic waves is too large to match the Bragg scattering scale size of 11 cm for the Sondrestrom radar. As a continuation of this work, a future study will look into the existence of enhanced plasma lines in the Sondrestrom data that coincide with dynamic, small-scale auroral structures. This could potentially put tighter bounds on the observability threshold of NEIALs with the Sondrestrom radar.

5. Conclusion

This case study comparison presented here is not definitive proof that NEIALs can never be observed with the Sondrestrom radar, but it does show that there is at least a very reduced sensitivity to scattering from the enhanced wave activity that exists inside such active aurora. The largely reduced NEIAL detectability of Sondrestrom is an advantage for accurately measuring polar cap boundary and substorm onset aurora, which cannot be accurately measured by PFISR because of the strong interference caused by the NEIAL backscatter.

This comparison shows that there is indeed a lack of NEIALs in the Sondrestrom data, when the geomagnetic conditions and visible aurorae are consistent with those that are known to occur with NEIALs in radar data from lower frequency radars. The location of Sondrestrom is ideally suited to frequently observe dynamic polar cap boundary aurora and therefore future auroral observing campaigns can be executed in order to continue the search for NEIALs in the Sondrestrom radar data.

The current data support the existence of a sharp cutoff in the scale size of the enhanced ion acoustic wave activity responsible for NEIALs in the 10 cm–15 cm range. They have been observed with Bragg scattering scale sizes between 16 cm and 67 cm with other radars, but to date they have not been observed at the 11 cm scale size of the Sondrestrom radar, indicating a largely reduced sensitivity to detecting NEIAL backscatter.

Acknowledgments

This work was supported by an internal research and development grant from the Southwest Research Institute Advisory Committee for Research. Support also comes from National Science Foundation Grant # AGS-1139135. The authors would like to thank SRI International, and specifically A. Strømme for assisting us in bringing our imagers to Sondrestrom. Thanks also to The University of Alaska, Fairbanks/Geophysical Institute for the use of their facilities and imagers at Poker Flat, AK, particularly D. Hampton for his assistance in imager operation.

References

- Akbari, H., Semeter, J.L., Dahlgren, H., Diaz, M., Zettergren, M., Strømme, A., Nicolls, M.J., Heinselman, C., 2012. Anomalous ISR echoes preceding auroral breakup: evidence for strong Langmuir turbulence. *Geophysical Research Letters* 39, 3102.
- Bahcivan, H., Cosgrove, R., 2008. Enhanced ion acoustic lines due to strong ion cyclotron wave fields. *Annales Geophysicae* 26, 2081–2095.
- Blixt, E.M., Grydeland, T., Ivchenko, N., Hagfors, T., La Hoz, C., Lanchester, B.S., Løvhaug, U.P., Trondsen, T.S., 2005. Dynamic rayed aurora and enhanced ion-acoustic radar echoes. *Annales Geophysicae* 23, 3–11.
- Cabrit, B., Opgenoorth, H., Kofman, W., 1996. Comparison between EISCAT UHF and VHF backscattering cross section. *Journal of Geophysical Research* 101, 2369–2376.
- Collis, P.N., Haggstrom, I., Kaila, K., Rietveld, M.T., 1991. EISCAT radar observations of enhanced incoherent scatter spectra and their relation to red aurora and field-aligned currents. *Geophysical Research Letters* 18, 1031–1034.
- Daldorff, L.K.S., Pécseli, H.L., Trulsen, J., 2007. Nonlinearly generated plasma waves as a model for enhanced ion acoustic lines in the ionosphere. *Geophysical Research Letters* 34, 18101.
- Forme, F.R.E., 1993. A new interpretation of the origin of enhanced ion acoustic fluctuations in the upper ionosphere. *Geophysical Research Letters* 20, 2347–2350.
- Forme, F.R.E., Fontaine, D., 1999. Enhanced ion acoustic fluctuations and ion outflows. *Annales Geophysicae* 17, 182–189.
- Foster, J.C., del Pozo, C., Groves, K., Saint Maurice, J.P., 1988. Radar observations of the onset of current driven instabilities in the topside ionosphere. *Geophysical Research Letters* 15, 160–163.
- Grydeland, T., Blixt, E., Løvhaug, U., Hagfors, T., La Hoz, C., Trondsen, T., 2004. Interferometric radar observations of filamented structures due to plasma instabilities and their relation to dynamic auroral rays. *Annales Geophysicae* 22, 1115–1132.
- Grydeland, T., La Hoz, C., Hagfors, T., Blixt, E.M., Saito, S., Strømme, A., Brekke, A., 2003. Interferometric observations of filamentary structures associated with plasma instability in the auroral ionosphere. *Geophysical Research Letters* 30, 1338.
- Guio, P., Forme, F., 2006. Zakharov simulations of Langmuir turbulence: effects on the ion-acoustic waves in incoherent scattering. *Physics of Plasmas* 13, 122902.
- Isham, B., Rietveld, M.T., Guio, P., Forme, F.R.E., Grydeland, T., Mjølhus, E., 2012. Cavitating Langmuir turbulence in the terrestrial aurora. *Physical Review Letters* 108, 105003 1101.3517.
- Kontar, E.P., Pécseli, H.L., 2005. Nonlinear wave interactions as a model for naturally enhanced ion acoustic lines in the ionosphere. *Geophysical Research Letters* 32, 5110.
- Lunde, J., Gustavsson, B., Løvhaug, U.P., Lorentzen, D.A., Ogawa, Y., 2007. Particle precipitations during NEIAL events: simultaneous ground based observations at Svalbard. *Annales Geophysicae* 25, 1323–1336.
- Mitchell, R.G., Lynch, K.A., Heinselman, C.J., Stenbaek-Nielsen, H.C., 2008. PFISR nightside observations of naturally enhanced ion acoustic lines, and their relation to boundary auroral features. *Annales Geophysicae* 26, 3623–3639.
- Mitchell, R.G., Lynch, K.A., Heinselman, C.J., Stenbaek-Nielsen, H.C., 2009. High time-resolution PFISR and optical observations of naturally enhanced ion-acoustic lines. *Annales Geophysicae* 27, 1457–1467.
- Mitchell, R.G., Samara, M., 2010. High-resolution observations of naturally enhanced ion acoustic lines and accompanying auroral fine structures. *Journal of Geophysical Research* 115.
- Ogawa, Y., Buchert, S.C., Fujii, R., Nozawa, S., Forme, F., 2006. Naturally enhanced ion-acoustic lines at high altitudes. *Annales Geophysicae* 24, 3351–3364.
- Ogawa, Y., Fujii, R., Buchert, S.C., Nozawa, S., Watanabe, S., van Eyken, A.P., 2000. Simultaneous EISCAT Svalbard and VHF radar observations of ion upflows at different aspect angles. *Geophysical Research Letters* 27, 81–84.
- Rees, M.H., 1963. Auroral ionization and excitation by incident energetic electrons. *Planetary and Space Science* 11, 1209.

- Rietveld, M.T., Collis, J.P., 1991. Naturally enhanced ion acoustic waves in the auroral ionosphere observed with the EISCAT 933-MHz radar. *Journal of Geophysical Research* 96, 19291–19305.
- Rietveld, M.T., Collis, P.N., Vaneyken, A.P., Løvhaug, U.P., 1996. Coherent echoes during EISCAT UHF Common Programmes. *Journal of Atmospheric and Terrestrial Physics* 58, 161–174.
- Sedgemore-Schulthess, K.J.F., Lockwood, M., Trondsen, T.S., Lanchester, B.S., Rees, M.H., Lorentzen, D.A., Moen, J., 1999. Coherent EISCAT Svalbard Radar spectra from the dayside cusp/cleft and their implications for transient field-aligned currents. *Journal of Geophysical Research* 104, 24613–24624.
- Strømme, A., Belyey, V., Grydeland, T., La Hoz, C., Løvhaug, U.P., Isham, B., 2005. Evidence of naturally occurring wave-wave interactions in the polar ionosphere and its relation to naturally enhanced ion acoustic lines. *Geophysical Research Letters* 32, 5103.